Journal of ELECTRONIC MATERIALS, Vol. 50, No. 4, 2021
https://doi.org/10.1007/s11664-020-08408-z

ASIAN CONSORTIUM ACCMS–INTERNATIONAL CONFERENCE ICMG 2020

Dielectric Relaxation Mechanism in High-Pressure Synthesized $BiCr_{0.5}Mn_{0.5}O_3$

P. MANDAL[1,2] and A. SUNDARESAN[1,3]

1.—School of Advanced Materials, Chemistry and Physics of Materials Unit, Jawaharlal Nehru Centre for Advanced Scientific Research, Jakkur P.O, Bangalore 560064, India. 2.—Department of Physics, SRM University – AP, Amaravati, Andhra Pradesh 522502, India. 3.—e-mail: sundaresan@jncasr.ac.in

The compound $BiCr_{0.5}Mn_{0.5}O_3$, synthesized at high pressure and high temperature, shows a giant dielectric constant over a wide range of temperatures. Two relaxation processes are observed commencing around 200 K and 300 K. The low-temperature relaxation process is attributed to Maxwell–Wagner polarization at the grain boundary, whereas the second relaxation is attributed to the electrode polarization effect. Impedance spectroscopy reveals that the oxide is electrically inhomogeneous and dominant contribution arises from semiconducting grains and insulating grain boundary below room temperature. Above room temperature, the electrode polarization effect also contributes to the observed giant dielectric constant.

Key words: Perovskite, high-pressure synthesis, giant dielectric constant, impedance spectroscopy, Maxwell–Wagner relaxation

INTRODUCTION

Dielectric materials are technologically demanding because of their use in various applications such as capacitors, sensors, actuators, resonators, filters, and memory devices. For practical applications, these materials require a high dielectric constant, low loss, and a constant value of permittivity in a broad temperature and frequency range.[1] High values of dielectric constant are observed in ferroelectric materials such as $BaTiO_3$ near the ferroelectric to paraelectric transition in a narrow temperature range. However, a large dielectric response has been reported in non-ferroelectric materials such as $CaCu_3Ti_4O_{12}$ (CCTO),[2–4] certain Fe-based compounds,[5,6] and other materials[4,7–11] in a broad temperature and frequency range. Earlier studies on polycrystalline CCTO samples showed that the origin of the giant dielectric constant was due to an intrinsic effect arising from slowing down of highly polarizable relaxational modes[2] or slowing down of dipolar fluctuations in nano-size domains.[3] Later, detailed studies on both polycrystalline and single-crystal samples indicated contributions from extrinsic effects,[12,13] and the mechanism is believed to be different in ceramic and single crystals.[14,15] Several mechanisms have been suggested in the literature; for example, Maxwell–Wagner-type relaxation either due to depletion layers at the grain boundaries or at the electrode–material interface.[8] In some systems, the internal barrier layer capacitance (IBLC) effect due to Schottky barrier formation at the grain boundaries best explains the giant dielectric constant in ceramics.[13,16] In single crystal of CCTO, the electrode polarization effect at the metal–semiconductor junction is believed to be responsible for such dielectric behavior.[8,14] In a few other materials, a colossal dielectric response is believed to be intrinsic, and the origin is attributed to electronic polarization.[4,6] From an application point of view, such high values of the dielectric constant should persist up to the gigahertz region, but most of these materials show a fall in the megahertz frequency.

(Received May 26, 2020; accepted August 11, 2020; published online August 19, 2020)

Recently, there has been considerable interest in bismuth-based perovskites of the type $BiMO_3$ (M = transition metals), which are potential candidates for materials exhibiting multiferroic properties.[17–20] Many of the bismuth compounds [$BiMO_3$ (where M = Cr, Mn, Co, or Ni)] require high pressures to stabilize the perovskite structure. For example, the high-pressure phase of $BiMnO_3$ is a widely studied material which has a monoclinic structure (C2/c) and shows ferromagnetic behavior with T_C of 100 K.[18] In fact, it has been reported that oxygen non-stoichiometry plays a crucial role in determining the structure and properties of $BiMnO_3$.[21] The compound $BiCrO_3$, which also has a centrosymmetric monoclinic structure (C2/c), exhibits a long-range G-type antiferromagnetic order (T_N = 109 K) with a weak ferromagnetic component.[22,23] However, these two compounds differ in their monoclinic angle, which is 110° and 108° for $BiMnO_3$ and $BiCrO_3$, respectively. Mixing of Mn and Cr ions in equal proportion at the B-site may give rise to interesting magnetic properties due to possible ordering of Cr and Mn ions. However, our recent study has shown that the compound $BiCr_{0.5}Mn_{0.5}O_3$ prepared by high-pressure synthesis is not an ordered perovskite and has structural and magnetic properties similar to $BiCrO_3$.[24] Surprisingly, it exhibits a giant dielectric constant over a wide range of temperatures (200–400 K). In the present article, we report a detailed relaxation mechanism characterized by dielectric and impedance studies. The origin of such a high dielectric constant is explained in terms of Maxwell–Wagner relaxation at the grain boundary and the electrode effect.

EXPERIMENTAL PROCEDURE

Polycrystalline $BiCr_{0.5}Mn_{0.5}O_3$ was synthesized using a cubic anvil type of apparatus at 1073 K and under a pressure of 4.5 GPa. Powder x-ray diffraction data were collected using a Bruker D8 Advance x-ray diffractometer, and phase purity was confirmed using Rietveld analysis using the FullProf software package as described elsewhere.[24] The density of the pellets used for dielectric measurements were 86-88% of the crystallographic density. Dielectric measurements were carried out with an impedance analyzer (Agilent 4294 A) using coaxial cable wire in a four-terminal pair–two-terminal configuration. Silver paint and DC sputtered gold was used as an electrode, and the capacitor was placed in a custom-made sample holder which was then inserted in the sample chamber of a cryo-cooled closed-cycle refrigerator system.

RESULTS AND DISCUSSION

Structure

X-ray diffraction data collected at room temperature confirms that the compound crystallizes in a monoclinic symmetry (C2/c) with lattice parameters a = 9.4645(3) Å, b = 5.5576(2) Å, c = 9.6524(3) Å, and β = 108.145(1)°. The Pawley fit to the x-ray data is shown in Fig. 1. A small amount (< 5%) of unidentified impurity was present as a secondary phase. Detailed structural properties are reported elsewhere.[24] It should be noted that the structure is centrosymmetric and does not allow ferroelectricity.

Dielectric Relaxation

Variation of dielectric constant (ε_r) and loss tangent (tan δ) at different frequencies in the temperature range of 20–400 K are shown in Fig. 2. The compound shows a giant value of dielectric constant (~ 14,000 at 1 kHz) and low loss (~ 0.95) at room temperature. Starting from low values (~ 100 below < 175 K), the dielectric constant data shows a large increase of around 200 K and a second anomaly around 300 K. Both the dielectric constant and loss data are highly frequency-dependent, and the peak position shifts toward higher temperature with increasing frequency. The two anomalies in the dielectric data correspond to two dielectric relaxations, which is more evident from the low-frequency dielectric constant [inset (i) of Fig. 2a] and low-frequency loss data (Fig. 2b). Interestingly, loss peaks corresponding to the first anomaly appear slightly at lower temperatures. On the other hand, the loss peaks corresponding to the second anomaly occur at higher temperatures. In addition to these two anomalies, high-temperature dielectric measurement showed a peak of around 650 K, reflecting the structural transition.[24] It should be noted here that $BiCrO_3$ shows dielectric anomalies at 440 K that are associated with (anti)ferroelectric to paraelectric transition. This transition coincides with the structural change from a monoclinic ($C2/c$) to orthorhombic ($Pnma$) structure.[22,23] In $BiCr_{0.5}Mn_{0.5}O_3$, the broad dielectric maxima near 200 K and 300 K are frequency-dependent, and

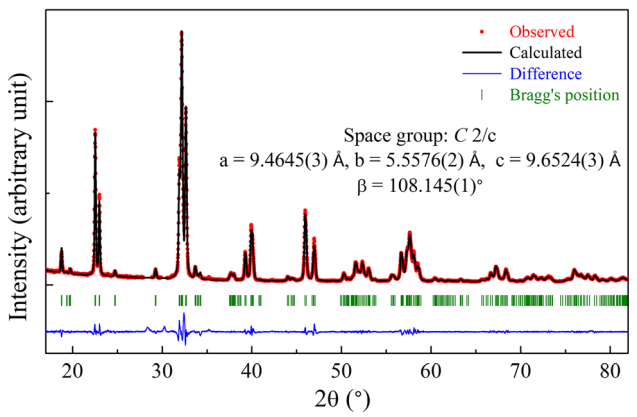

Fig. 1. Pawley fit to the room-temperature powder x-ray data using monoclinic structure space group C2/c. Red dots represent the observed data, black line indicates calculated pattern, the blue line shows the difference between observed and calculated values and the green ticks represent Bragg's position (Color figure online).

there is no structural change around this temperature range.[24] Therefore, these dielectric anomalies do not correspond to structural transition or ferroelectric-to-paraelectric transition. The first relaxation seems to be due to a Maxwell–Wagner type of relaxation at the grain boundary where the surface charges pile up at the interface due to the difference in conductivity at the grain and grain boundary regions upon application of an AC bias and give rise to Debye-like relaxation behavior. This phenomenon is commonly observed in several electrically inhomogeneous systems in which the giant dielectric constant appears around 200 K.[5,7,25]

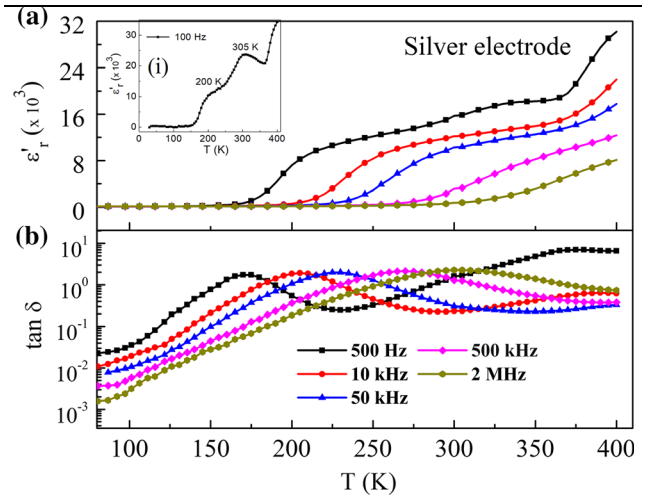

Fig. 2. Temperature dependence of (a) relative dielectric constant (ε_r), and (b) loss (tan δ) plotted for different frequencies. Inset (i) shows dielectric constant data at low frequency (100 Hz)

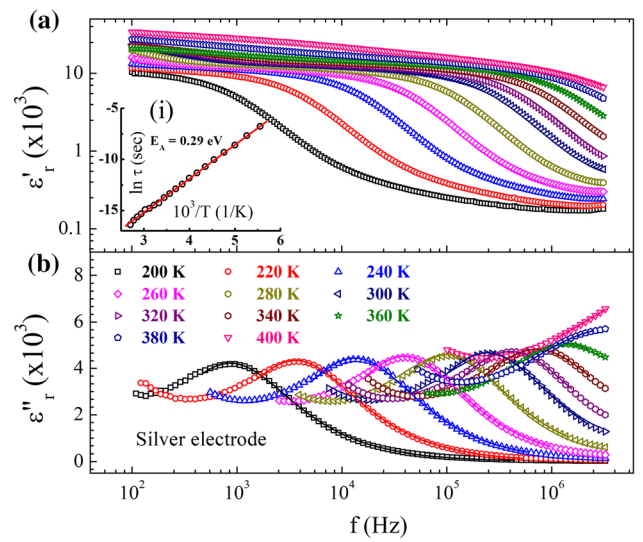

Fig. 3. Variation of the (a) real (ε_r') and (b) imaginary (ε_r'') parts of the dielectric constant as a function of frequency at different temperatures. Data has been plotted for selected temperatures for clarity. Solid lines in (b) represent fits to modified Debye relation (see text). The inset shows relaxation time (τ), which follows the Arrhenius equation for the activated process

Figure 3 shows the real and imaginary parts of the dielectric constant plotted against frequency at different temperatures. At low frequency, the real part shows a plateau and then decreases dramatically to a constant low value of $\varepsilon_r' \sim 500$ at high frequencies. It should be noted that this constant value of ε_r at high frequency is still higher than the intrinsic dielectric constant of a material. The step-like behavior of ε_r with a coinciding peak in the loss spectra (Fig. 3b) is typical of a Debye-like relaxation process. However, we found that the behavior deviates from the ideal Debye relaxation which assumes a single relaxation time (τ).[26] The behavior was found to follow the modified Debye relation which includes a distribution of relaxation times defined by a parameter α.[27] The dielectric constant was fitted with equation $\varepsilon^*(\omega) = \varepsilon_\infty + (\varepsilon_0 - \varepsilon_\infty)/(1 + (\iota\omega\tau)^{1-\alpha})$ where ε_0 and ε_∞ are the low- and high-frequency dielectric constants, and $\alpha \to 0$ gives the typical Debye relaxation behavior. The solid lines in Fig. 3b through the points show fit to the ε_r'' using the modified Debye relation. From the fitting, the obtained value of α vary from 0.13 to 0.58 with temperature. The most probable relaxation times, extracted from the fit, follow Arrhenius' law $\tau = \tau_0 e^{-E_A/k_B T}$ with an activation energy of 0.29 eV.

Conductivity Analysis

To understand the high-temperature relaxation process, AC conductivity ($\sigma^* = j\omega\varepsilon^*$), calculated from the dielectric data, was analyzed in the temperature range 300–400 K. Figure 4 shows the real part of conductivity ($\sigma' = \omega\varepsilon_0\varepsilon''$) plotted against frequency at different temperatures. At high temperatures, AC conductivity values become nearly independent in the low-frequency region. This observation excludes the possibility of pure ionic conduction in the material. It is well known that electrical response in an inhomogeneous ceramic

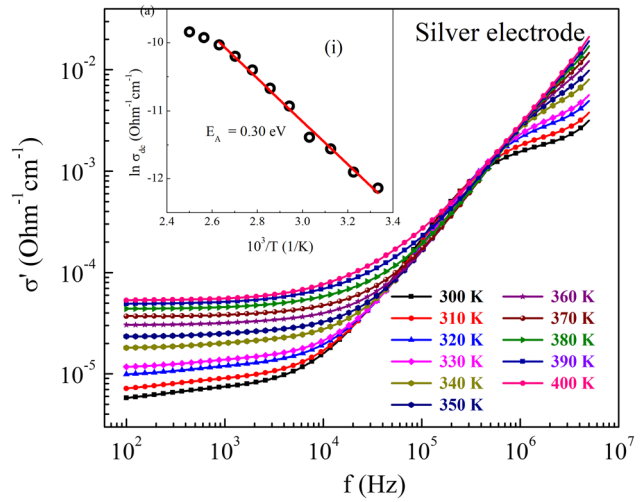

Fig. 4. Real parts of AC conductivity (σ') against frequency shown at different temperatures. Inset shows DC conductivity derived from the AC conductivity plot, following the Arrhenius equation

consists of various electroactive regions such as semiconducting grain and insulating grain boundary. The resistivity at low frequency in Fig. 4 corresponds to the more resistive component in an electrically inhomogeneous ceramic. The DC conductivity values were extracted at each temperature by extrapolating AC conductivity (σ') to zero frequency. The obtained DC conductivity (Fig. 4 inset) follows Arrhenius behavior with an activation energy of 0.30 eV. This value is comparable to the activation energy associated with the DC conduction in mixed valent Mn compounds.[25,28]

Impedance Study

The dielectric data can be analyzed using impedance spectroscopy, which allows us to relate the electrical properties to its microstructure and also to separate the contributions from different electroactive regions. Figure 5 shows the Nyquist or Z^* (Z'' versus Z') plot at 250 K, where parts of two semicircular arcs indicate that the electrical response is dominated by mainly two contributions, each of which can be represented by a parallel capacitance (C)–resistance (R) component. This is also corroborated by Z'', M'' versus f plots (not shown here). Capacitance values extracted from Z^* plots in the high- and low-frequency arcs are of the order of pF and nF (22.2 pF and 0.56 nF at 250 K), which correspond to grain and grain boundary values.[29] The extracted values of the grain and grain boundary resistance are R_b = 11.4 kΩ and R_{gb} = 2.28 MΩ at 250 K, respectively. The semiconducting nature of grains and insulating nature of the grain boundary are common in electrically inhomogeneous ceramics.[8,13,30–33] Both grain and grain boundary resistance values extracted from the circular fit were found to follow Arrhenius law with close activation energies of 0.27 eV. This behavior may indicate that the grain boundary response is associated with the constriction resistance, which occurs due to the necking of grains, possibly due to lower pellet density, which gives rise to similar behavior of grain and grain boundary resistance. This activation energy is also close to that of the low-temperature dielectric relaxation.

Above 270 K, the low-frequency arc (grain boundary contribution) deviates from the semicircular shape, which may indicate presence of other extrinsic contributions. This was assessed by measuring dielectric constant with different thicknesses (400–275 μm) and different electrodes from sputtered gold to silver paint, as shown in Fig. 5b. The corresponding impedance data are shown in Fig. 6. The low-frequency region (< 100 kHz) shows a large difference both in the thickness dependence experiment (Fig. 6a) and the electrode dependence experiment (Fig. 6b). The electrode dependence experiment was aimed to evaluate the effect of electrode materials with different electron work functions. The dielectric constant values are different in the low-frequency region, but they merge at high frequencies, which suggests contributions from extrinsic factors such as interfacial polarization or an electrode polarization effect.[13] In several oxides such as CuO and $CaCu_3Ti_4O_{12}$, the low-frequency dielectric response is reported to be dependent on the electrode materials and the thickness.[13,30,31] This has been attributed to the interfacial polarization or electrode effect at the non-Ohmic contacts between a metal electrode and semiconductor due to formation of Schottky barriers.[13,30,31] The large difference in dielectric behavior with electrode material can be explained as follows. $BiCr_{0.5}Mn_{0.5}O_3$ is possibly an n-type semiconductor. In semiconducting oxides, the electrodes, e.g., Au with high electron work function (5.1 eV), can produce a non-Ohmic contact or Schottky barriers at the electrode–ceramic interface. This effect is known to result in a large dielectric constant and has been observed in several inhomogeneous oxides such as the n-type $BaTiO_3$. Interestingly, the dielectric constant of $BiCr_{0.5}Mn_{0.5}O_3$ is lower for a silver electrode compared to a gold electrode. The electron

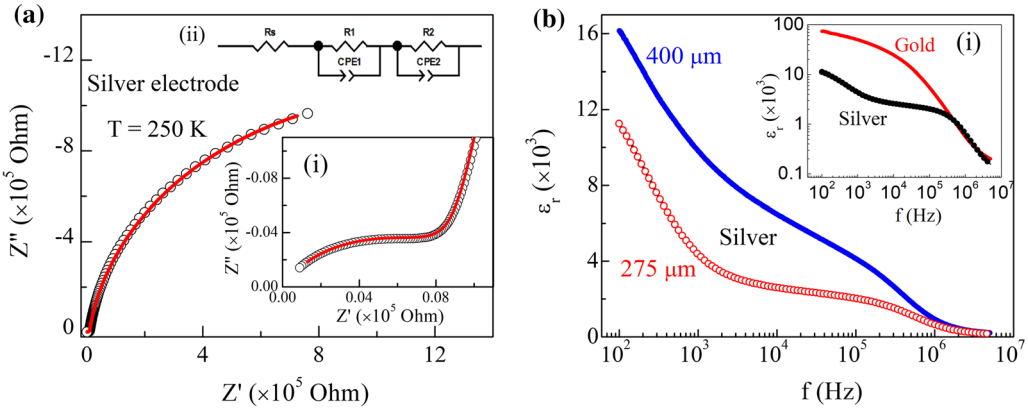

Fig. 5. (a) Nyquist plot at 250 K showing experimental data (open circle) and simulated data (solid line) using an equivalent circuit shown in the inset a(ii). Inset a(i) shows the high-frequency region zoomed for clarity. (b) Dielectric constant versus frequency at room temperature for samples with thickness of 400 μm (blue line) and 275 μm (red circle). Inset b(i) shows the behavior for different electrode materials; black circles and the red line correspond to silver (paint) and gold (sputtered) electrodes, respectively (Color figure online).

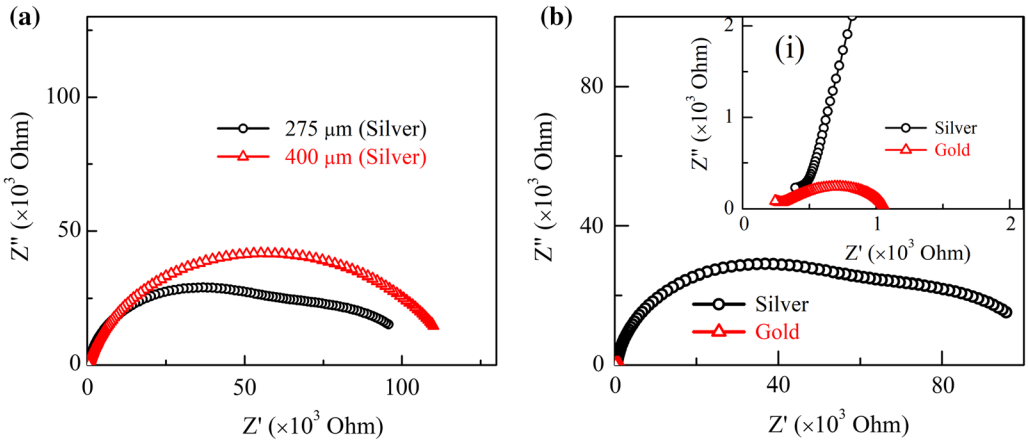

Fig. 6. Nyquist plots at 300 K corresponding to dielectric data presented in Fig. 5b. (a) Z'' versus Z' plots for a sample thickness of 400 μm (red triangles) and 275 μm (black circles). Silver paste was used as the electrode. (b) Z'' versus Z' plots for the silver electrode (black circles) and sputtered gold electrode (red triangles) using pellets of similar thickness. Inset (i) shows high-frequency region zoomed for clarity (Color figure online).

work function of silver ($\sim$ 4.3 eV) is lower compared to the work function of gold,[13,30,31] and hence a lower dielectric constant is observed (Fig. 5b).

Electrode contribution plays a significant role above 280 K, whereas at lower temperature, the Nyquist plots (Fig. 5a) reveal contributions from the grains and grain boundary. Based on the following observations, an equivalent circuit was proposed to model the impedance data at 250 K, as shown in the inset (ii) of Fig. 5a, excluding the electrode effect. The resistance R_s is assigned to account for the non-zero intercept of the high-frequency arc to the real axis, and capacitance is replaced with a constant-phase element (CPE; $Z_{CPE} = 1/C_n(i\omega)^n$), where C_n is an independent frequency term which acts like capacitance value, and n signifies the deviation from the ideal capacitor behavior.[34] Simulated data (shown by solid lines in Fig. 5a) at 250 K using the above-mentioned equivalent circuit shows a good agreement with the experimental data. Inset (i) in Fig. 5a shows the same result zoomed in the high-frequency region. The values of n obtained for low- and high-frequency regions are 0.76 and 0.93, respectively. The high-frequency value is close to unity, which reflects the internal effects.

CONCLUSIONS

The material $BiCr_{0.5}Mn_{0.5}O_3$ exhibits a giant dielectric constant in a broad temperature range with two relaxations. The low-temperature relaxation process is explained using Maxwell–Wagner polarization at the grain boundary, whereas the relaxation at higher temperature is attributed to the electrode polarization effect or interfacial polarization. Impedance studies show that the low-temperature dielectric response in the electrically inhomogeneous ceramics is dominated by grain and grain boundary contributions. At higher temperatures, contribution from the electrode effect was observed in the low-frequency region. A good agreement was obtained between experimental and simulated data using a proposed equivalent circuit.

ACKNOWLEDGMENTS

A.S. would like to acknowledge the financial support from the Science and Engineering Board (SERB sanction No. CRG/2018/000520), Department of Science and Technology (DST), Government of India.

CONFLICT OF INTEREST

The authors declare that they have no conflict of interest.

REFERENCES

1. R.J. Cava, *J. Mater. Chem.* 11, 54 (2001).
2. A.P. Ramirez, M.A. Subramanian, M. Gardel, G. Blumberg, D. Li, T. Vogt, and S.M. Shapiro, *Solid State Commun.* 115, 217 (2000).
3. C.C. Homes, T. Vogt, S.M. Shapiro, S. Wakimoto, and A.P. Ramirez, *Science* 293, 673 (2001).
4. M.M. Ahmad and K. Yamada, *Appl. Phys. Lett.* 91, 052912 (2007).
5. I.P. Raevski, S.A. Prosandeev, A.S. Bogatin, M.A. Malitskaya, and L. Jastrabik, *J. Appl. Phys.* 93, 4130 (2003).
6. N. Ikeda, H. Ohsumi, K. Ohwada, K. Ishii, T. Inami, K. Kakurai, Y. Murakami, K. Yoshii, S. Mori, Y. Horibe, and H. Kito, *Nature* 436, 1136 (2005).
7. J. Liu, C. Duan, W.N. Mei, R.W. Smith, and J.R. Hardy, *J. Appl. Phys.* 98, 093703 (2005).
8. P. Lunkenheimer, V. Bobnar, A.V. Pronin, A.I. Ritus, A.A. Volkov, and A. Loidl, *Phys. Rev. B* 66, 052105 (2002).
9. P. Gupta, P.K. Mahapatra, and R.N.P. Choudhary, *J. Phys. Chem. Solids* 137, 109217 (2020).
10. S. Chatterjee, R. Maiti, and D. Chakravorty, *RSC Adv.* 10, 13708 (2020).
11. C.M. Zhu, G.B. Yu, L.G. Wang, M.W. Yao, F.C. Liu, and W.J. Kong, *J. Magn. Magn. Mater.* 506, 166803 (2020).
12. L. He, J.B. Neaton, M.H. Cohen, D. Vanderbilt, and C.C. Homes, *Phys. Rev. B* 65, 214112 (2002).
13. P. Lunkenheimer, R. Fichtl, S.G. Ebbinghaus, and A. Loidl, *Phys. Rev. B* 70, 172102 (2004).
14. M.H. Cohen, J.B. Neaton, L. He, and D. Vanderbilt, *J. Appl. Phys.* 94, 3299 (2003).

15. S. Krohns, P. Lunkenheimer, S.G. Ebbinghaus, and A. Loidl, *Appl. Phys. Lett.* 91, 022910 (2007).
16. D.C. Sinclair, T.B. Adams, F.D. Morrison, and A.R. West, *Appl. Phys. Lett.* 80, 2153 (2002).
17. J. Wang, J.B. Neaton, H. Zheng, V. Nagarajan, S.B. Ogale, B. Liu, D. Viehland, V. Vaithyanathan, D.G. Schlom, U.V. Waghmare, N.A. Spaldin, K.M. Rabe, M. Wuttig, and R. Ramesh, *Science* 299, 1719 (2003).
18. T. Kimura, S. Kawamoto, I. Yamada, M. Azuma, M. Takano, and Y. Tokura, *Phys. Rev. B* 67, 180401 (2003).
19. C. De, Á.M. Arévalo-López, F. Orlandi, P. Manuel, J.P. Attfield, and A. Sundaresan, *Angew. Chem. Int. Ed.* 57, 16099 (2018).
20. P. Mandal, M.J. Pitcher, J. Alaria, H. Niu, P. Borisov, P. Stamenov, J.B. Claridge, and M.J. Rosseinsky, *Nature* 525, 363 (2015).
21. A. Sundaresan, R.V.K. Mangalam, A. Iyo, Y. Tanaka, and C.N.R. Rao, *J. Mater. Chem.* 18, 2191 (2008).
22. A.A. Belik, S. Iikubo, K. Kodama, N. Igawa, S. Shamoto, and E. Takayama-Muromachi, *Chem. Mater.* 20, 3765 (2008).
23. S. Niitaka, M. Azuma, M. Takano, E. Nishibori, M. Takata, and M. Sakata, *Solid State Ion.* 172, 557 (2004).
24. P. Mandal, A. Iyo, Y. Tanaka, A. Sundaresan, and C.N.R. Rao, *J. Mater. Chem.* 20, 1646 (2010).
25. Y.Q. Lin, Y.J. Wu, X.M. Chen, S.P. Gu, J. Tong, and S. Guan, *J. Appl. Phys.* 105, 054109 (2009).
26. P. Debye, *Polar Molecules* (New Work: Chemical Catalogue Company, 1929).
27. K.S. Cole and R.H. Cole, *J. Chem. Phys.* 9, 341 (1941).
28. C.C. Wang, Y.M. Cui, and L.W. Zhang, *Appl. Phys. Lett.* 90, 012904 (2007).
29. J.T.S. Irvine, D.C. Sinclair, and A.R. West, *Adv. Mater.* 2, 132 (1990).
30. M. Li, A. Feteira, and D.C. Sinclair, *J. Appl. Phys.* 105, 114109 (2009).
31. M. Li, Z. Shen, M. Nygren, A. Feteira, D.C. Sinclair, and A.R. West, *J. Appl. Phys.* 106, 104106 (2009).
32. T.B. Adams, D.C. Sinclair, and A.R. West, *Phys. Rev. B* 73, 094124 (2006).
33. F.D. Morrison, D.C. Sinclair, and A.R. West, *J. Am. Ceram. Soc.* 84, 531 (2001).
34. E. Barsoukov and MacDonald JR, eds., *Impedance Spectroscopy: Theory, Experiment and Applications* (New York: Wiley Interscience, 2005).